*Journal of the Korean Society for Nondestructive Testing*
*Vol. 28, No. 6 (2008. 12)*

# Numerical Evaluation of Phase Velocity and Attenuation of Ultrasonic Waves in Fiber-Reinforced Composites Using the Mass-Spring-Dashpot Lattice Model

Eunsol Baek* and Hyunjune Yim*†

**Abstract** The paper presents a numerical study to evaluate the phase velocities and attenuations of the average longitudinal and shear ultrasonic waves resulting from multiple scattering in fiber-reinforced composites. A computational procedure developed in this work is first used to produce a random, yet largely even distribution of fibers. Both the viscoelastic epoxy matrix and lossless randomly distributed graphite fibers are modeled using the mass-spring-dashpot lattice model, with no damping for the latter. By numerically simulating ultrasonic through-transmission tests using this direct model of composites, phase velocities and attenuations of the longitudinal and shear waves through the composite are found as functions of frequency or fiber concentration. The numerical results are observed to generally agree with the corresponding results in the literature. Discrepancies found in some detail aspects, particularly in the attenuation results, are also addressed.

**Keywords:** Numerical Simulation, Ultrasonic Testing, Fiber Composite, Phase Velocity, Attenuation, Mass-Spring-Dashpot Lattice Model

## 1. Introduction

Multiple scattering of ultrasonic waves in fiber-reinforced composite materials has long been a subject of active research in the area of nondestructive testing with the continuing increase of their structural applications. Researchers developed a number of analytical and numerical models for this complex wave phenomenon. Most research papers found in the literature are about the two-dimensional wave phenomena in the plane perpendicular to the axial direction of unidirectional fibers, rendering fibers modeled as identical circular scatterers. One of the earliest and classical models is based on the method of wave-function series expansion to express both incident and scattered waves for each circular scatterer or fiber (Pao and Mow, 1963). As the number of fibers increases, such analytical model could not then be used because of the prohibitively increasing amount of computation. This approach has recently been revisited owing to the great advancement of the computing power available. One such example is the recent research by Biwa et al. (2004). They used the same method of wave-function expansion to evaluate the effective material properties of the composite by taking the average of wavefields over various random configurations of the fibers.

Besides the analytical method of wave-function expansion, several different groups of research have been conducted to simulate the average waves through the composite medium, which provide information on the effective material properties. The first group of such research includes Foldy (1945), Waterman and

Received: October 22, 2008, Revised: December 1, 2008, Accepted: December 3, 2008. * Hongik University, Department of Mechanical Engineering, Seoul, 121-791, Korea † Corresponding Author: hjyim@hongik.ac.kr

Truell(1961), and Twersky(1962a, 1962b). They made several assumptions on the probabilistic distribution and relative positions of the fibers, and obtained the configurational average of the ultrasonic waves through the medium. Later, Sayers(1980), Sayers and Smith (1983), and Datta et al. (1988) applied the same approach to particle-reinforced composites. This class of research, including both the early and later groups, were limited mostly to the cases of low volume fraction (or concentration) of reinforcements, or to the limiting cases of independent single scattering.

In order to overcome this limitation, Bose and Mal (1973, 1974), Varadan et al. (1978, 1986), and Willis (1980a, 1980b) introduced a hypothetical concept of pair correlation function that describes specific probability functions for the relative positions of any two fibers. Incorporating this pair correlation function in the model enabled to consider the fundamental wave interactions between fibers, but did not always yield physically viable results for high fiber concentration.

Another noteworthy model for wave characteristics of composites is the generalized self-consistent model (GSCM) proposed by Christensen and Lo (1979). This hypothetical model is particularly concerned with assessing the material properties of the composite's effective medium that is defined as a homogeneous material equivalent to the (inhomogeneous) composite from the perspective of wave propagation. The GSCM first assumes that embedded in a background medium of unknown properties is a single circular inclusion that consists of a circular core made of the fiber material and a surrounding shell made of the matrix material. The radius of the core and the thickness of the shell are determined according to the fiber concentration of the composite. Then, the GSCM argues that there will be no scattering if the background medium is indeed the effective medium of the composite; thus, it finds the material properties of the background medium that yields no wave scattering, and suggests them as the effective medium's average material properties. Though the overall concept of the GSCM seems reasonable, it is not clear whether the hypothetical model could capture all the complex wave interactions in multiple scattering that occur in the fiber-reinforced composite.

The present paper attempts to numerically find the characteristics of the average wave through a fiber-reinforced composite in a manner similar to Biwa et al. (2004). The similarity lies in that all fibers are actually modeled and distributed randomly as they are in real situations, and thus the realistic wave interactions between the fibers are all taken into account. Therefore, this type of approach may fall in the category of so called *direct* modeling of physical phenomena. A major difference, however, is that the present work uses a numerical model whereas Biwa et al. (2004) is based on the analytical model of Pao and Mow (1963). Though the difference may seem trivial, the consequences are not. This is because the numerical modeling used in the present work offers greater flexibility and ease in modeling various anomalies such as cracks and inclusions embedded in the composite, which is important in nondestructive testing of composite materials particularly in structural applications.

## 2. Modeling of Fiber-Reinforced Composite

### 2.1. Constituents of Composite

The material considered in this work is a graphite-epoxy composite. It is assumed that the epoxy matrix exhibits linear viscoelasticity while the graphite fibers linear elasticity, and that both phases are homogeneous. The material properties of the two phases used in this work are listed in Table 1, mostly following Yang and Mal (1994). Note that $\Pi$, called the instantaneous modulus governing longitudinal waves, and M, called the

instantaneous modulus governing shear waves, in Table 1 are generic elastic constants that can be used for both elastic and viscoelastic materials, as explained in Thomas (2006). The dispersion coefficient, $r$, in Table 1 represents the extent of dispersion in the standard linear model, the most widely accepted model for viscoelastic materials (Kolsky, 1963). For the problem at hand, the generic elastic moduli, Π and M, are related to the Lamè constants via simple equations: $\lambda = r(\Pi - 2M)$, $\mu = rM$ (Thomas, 2006). Further, the attenuation coefficient of epoxy, given in Table 1, means the attenuation $\alpha$ at the frequency of 1 MHz (Dorighi et al., 1997).

## 2.2. Distribution of Fibers

Fig. 1 shows a schematic diagram of a typical distribution of fibers in composites. In this work, assuming that all fibers are of an identical size and are perfectly aligned, they are modeled as identical circles in the $x$-$y$ plane as shown in Fig. 1.

In order to distribute fibers in a rectangular domain of the numerical model, the number of fibers commensurate with a desired fiber concentration is first determined. Then, the fibers are placed one after another, at discrete locations, i.e. the nodes of a square lattice of the numerical model to be explained in Section 2.3, within the predetermined rectangular domain. The fiber placement scheme consists of two

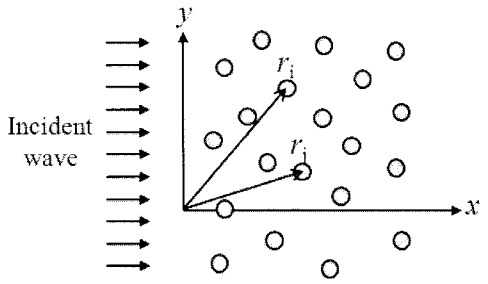


Fig. 1 Distribution of fibers

steps. The first step is to use a random number generator to obtain two random whole numbers within preset ranges, which correspond to the $x$ and $y$ indices of the lattice node where the fiber would be placed. The second step is to check if the center of the new fiber to be placed, i.e. the randomly selected node in the first step, is not within a predetermined distance from the center of any other preexisting fiber. This predetermined distance, $d$, of mutual exclusion of fiber centers was set in this work as

$$d = 2a\left(1 + \frac{1}{10c}\right) \tag{1}$$

where $a$ is the fiber radius and c is the desired fiber concentration. Eqn. (1) has been developed somewhat arbitrarily in this work such that (a) the fibers are randomly but rather evenly distributed, i.e. not very dense in a region and very sparse in another, and (b) the fiber placement does not take too long a computer time. The former consideration, (a), is consistent with the special attention usually paid in real

Table 1 Material properties of matrix and fiber (Yang and Mal, 1994)

| Properties | Matrix (epoxy) | Fiber (graphite) |
|---|---|---|
| Elastic constant, Π [GPa] | 5.504 | 15.0 |
| Elastic constant, M [GPa] | 1.98 | 5.02 |
| Dispersion coefficient, $r$ | 0.698 | 1.0 |
| Poisson's ratio | 0.353 | 0.29 |
| Density [kg/m$^3$] | 1260 | 1790 |
| Longitudinal phase velocity, $c_p$ [m/s] | 2060.6 | 2895 |
| Shear phase velocity, $c_s$ [m/s] | 1253.6 | 1675 |
| Attenuation coefficient [dB/cm at 1 MHz] | 2.0 | — |

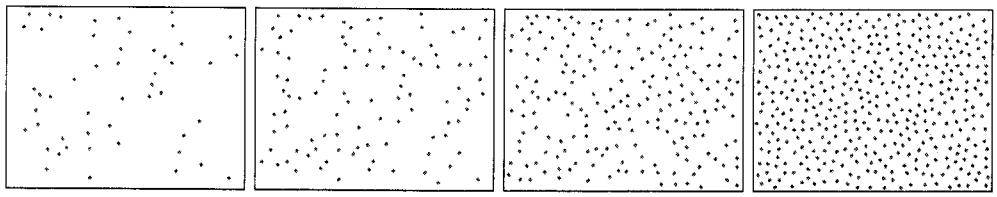

Fig. 2 Fiber distributions at successive stages of fiber placement process

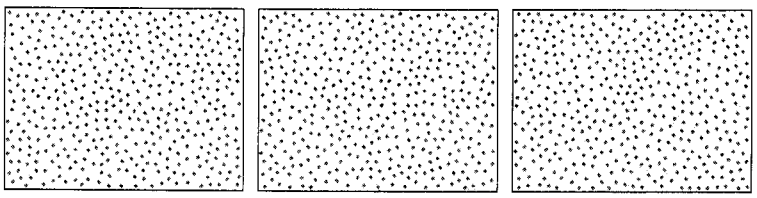

Fig. 3 Examples of fiber distributions having identical concentration

fabrication of composites to evenly distribute the fibers. If the fiber being placed does not satisfy this requirement of inter-fiber separation, the first step is conducted again to reselect its new location and then the second step is performed to see if this new location is acceptable. This procedure is continued until the fiber is placed at an acceptable location; further, it is repeated until all fibers are placed. Therefore, the resulting fiber distribution will guarantee that any pair of fibers, for example the $i$th and $j$th fibers in Fig. 1, satisfies

$$\left|\mathbf{r}_i - \mathbf{r}_j\right| \geq d \qquad \forall i \neq j \tag{2}$$

Fig. 2 shows fiber distributions captured at four successive stages of the process described above, for a fiber concentration of 0.1 and a square domain of 400 x 300 nodes. It can be observed that the fiber distribution becomes more and more uniform as the fiber placement progresses. Also, Fig. 3 shows three examples of finally obtained fiber distributions for an identical fiber concentration of 0.1. All three examples shown in Fig. 3 look similar to each other, mainly because of the requirement given by eqns. (1) and (2). As a result, it was found that such different distributions of fibers at an identical fiber concentration exhibit virtually same wave characteristics, at least in terms of the phase velocities and attenuations studied in this work. Therefore, in this work, only one distribution has been used for a single fiber concentration, without considering different distributions and taking configurational averages, to substantially save computation time.

### 2.3. Numerical Models - MSLM and MSDLM

Numerical models used in the present work are the mass-spring lattice model (MSLM) and the mass-spring-dashpot lattice model (MSDLM). The MSLM is a model for linearly elastic material which uses masses, distributed in a square lattice with the horizontal and vertical lattice spacing $h$, interconnected through linear springs (see Fig. 4(a)). It has been used in many recent simulation studies of various ultrasonic nondestructive evaluation problems (Yim and Sohn, 2000; Yim and Choi, 2000; Yim and Lee, 2002; Yim and Baek, 2002, 2004; Baek and Yim, 2004; Baek, 2007). Note that the MSLM shown in Fig. 4(a) is used in the present work to obtain the reference signal for the estimation of the attenuation of the composite material (see Sections 3.2 and 4.2).

The MSDLM, on the other hand, is a model that was more recently developed by adding dashpots to the MSLM (Thomas, 2006) as shown in Fig. 4(b). In Fig. 4(b), $g_i$'s denote extensional spring constants, $b_i$'s the extensional dashpot coefficients, $\eta_i$'s the rotational spring constants, and $\gamma_i$'s the rotational dashpot

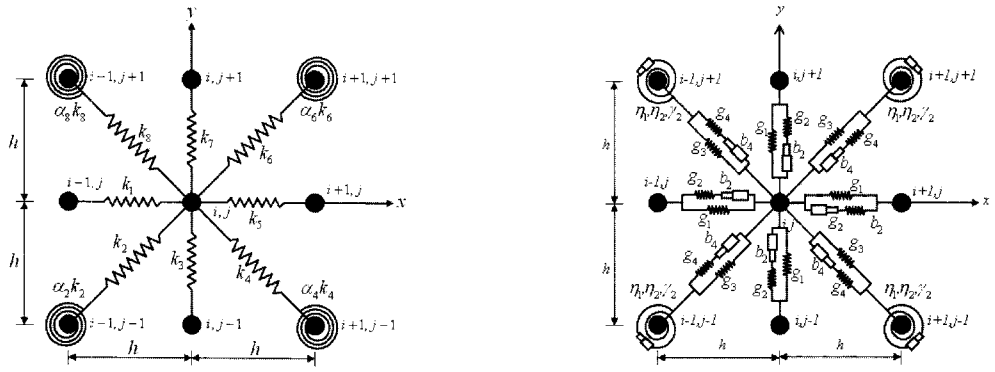

(a) (b)

Fig. 4 Numerical models used: (a) MSLM, (b) MSDLM

coefficients. Note in Fig. 4(b) that both the linear and the rotational spring-dashpot combinations contain one spring juxtaposed with one spring-dashpot series, as in the widely accepted viscoelastic model called the standard linear solid model (Kolsky, 1963).

Due to the dashpots introduced into the model, the MSDLM can model viscous effects in addition to the inertial and elastic effects modeled by the mass and springs as in the MSLM. The difference equations used for computations of the MSDLM may be obtained by establishing the equations of motion for a mass, e.g. the center mass in Fig. 4(b), in terms of its relative displacement and velocity with respect to the neighboring masses, as

$$\begin{aligned}\frac{df^x_{i,j}}{dt} &= -\frac{1}{\tau}f^x_{i,j} + \frac{g_1}{\tau h^2}\left(u_{i+1,j} - 2u_{i,j} + u_{i-1,j}\right) + \frac{1}{\tau h^2}\left(\frac{g_3}{2} + \frac{\eta_1}{4h^2}\right)\left(u_{i+1,j+1} + u_{i-1,j-1} + u_{i+1,j-1} + u_{i-1,j+1} - 4u_{i,j}\right)\\ &+ \frac{1}{\tau h^2}\left(\frac{g_3}{2} - \frac{\eta_1}{4h^2}\right)\left(v_{i+1,j+1} + v_{i-1,j-1} - v_{i+1,j-1} - v_{i-1,j+1}\right) + \left(\frac{g_1+g_2}{h^2}\right)\left(\dot{u}_{i+1,j} - 2\dot{u}_{i,j} + \dot{u}_{i-1,j}\right)\\ &+ \frac{1}{h^2}\left(\frac{g_3+g_4}{2} + \frac{\eta_1+\eta_2}{4h^2}\right)\left(\dot{u}_{i+1,j+1} + \dot{u}_{i-1,j-1} + \dot{u}_{i+1,j-1} + \dot{u}_{i-1,j+1} - 4\dot{u}_{i,j}\right)\\ &+ \frac{1}{h^2}\left(\frac{g_3+g_4}{2} - \frac{\eta_1+\eta_2}{4h^2}\right)\left(\dot{v}_{i+1,j+1} + \dot{v}_{i-1,j-1} - \dot{v}_{i+1,j-1} - \dot{v}_{i-1,j+1}\right)\end{aligned} \tag{3}$$

$$\begin{aligned}\frac{df^y_{i,j}}{dt} &= -\frac{f^y_{i,j}}{\tau} + \frac{g_1}{\tau h^2}\left(v_{i,j+1} - 2v_{i,j} - v_{i,j-1}\right) + \frac{1}{\tau h^2}\left(\frac{g_3}{2} + \frac{\eta_1}{4h^2}\right)\left(v_{i+1,j+1} + v_{i-1,j-1} + v_{i+1,j-1} + v_{i-1,j+1} - 4v_{i,j}\right)\\ &+ \frac{1}{\tau h^2}\left(\frac{g_3}{2} - \frac{\eta_1}{4h^2}\right)\left(u_{i+1,j+1} + u_{i-1,j-1} - u_{i+1,j-1} - u_{i-1,j+1}\right) + \frac{g_1+g_2}{h^2}\left(\dot{v}_{i,j+1} - 2\dot{v}_{i,j} - \dot{v}_{i,j-1}\right)\\ &+ \frac{1}{h^2}\left(\frac{g_3+g_4}{2} + \frac{\eta_1+\eta_2}{4h^2}\right)\left(\dot{v}_{i+1,j+1} + \dot{v}_{i-1,j-1} + \dot{v}_{i+1,j-1} + \dot{v}_{i-1,j+1} - 4\dot{v}_{i,j}\right)\\ &+ \frac{1}{h^2}\left(\frac{g_3+g_4}{2} - \frac{\eta_1+\eta_2}{4h^2}\right)\left(\dot{u}_{i+1,j+1} + \dot{u}_{i-1,j-1} - \dot{u}_{i+1,j-1} - \dot{u}_{i-1,j+1}\right)\end{aligned} \tag{4}$$

$$\frac{du_{i,j}}{dt} = \dot{u}_{i,j} \tag{5}$$

$$\frac{dv_{i,j}}{dt} = \dot{v}_{i,j} \tag{6}$$

$$\frac{d\dot{u}_{i,j}}{dt} = \frac{1}{\rho}\left(f^{bx}_{i,j} + f^x_{i,j}\right) \tag{7}$$

$$\frac{d\dot{v}_{i,j}}{dt} = \frac{1}{\rho}\left(f^{by}_{i,j} + f^y_{i,j}\right) \tag{8}$$

where the subscripts denote the indices of masses as shown in Fig. 4(b); $u$ and $v$ are displacements in the $x$ and $y$ directions, respectively; and, $f^x$ and $f^y$are forces in the $x$ and $y$ directions, respectively, exerted by springs and dashpots whereas $f^{bx}$ and $f^{by}$ are body forces. Unlike the MSLM, relative velocities of where the subscripts denote the indices of masses as shown in Fig. 4(b); $u$ and $v$ are displacements in the $x$ and $y$ directions, respectively; and, $f^x$ and $f^y$are forces in the $x$ and $y$ directions, respectively, exerted by springs and dashpots whereas $f^{bx}$ and $f^{by}$ are body forces. Unlike the MSLM, relative velocities of masses are also involved in the MSDLM difference equations, as may be seen from eqns. (3) through (8), which need to be integrated with respect to time. Thus, the Runge-Kutta numerical integration scheme is used as in Thomas (2006).

The mass, spring constants, and dashpot parameters of the MSDLM shown in Fig. 4(b) and contained in eqns. (3) through (8) may be determined by requiring that the difference equations be consistent with the stress-dynamic equations of motion of the medium at hand. The thus obtained relationships are given as

$$g_1 = r(\Pi - \mathrm{M}) \tag{9}$$

$$g_2 = (1-r)(\Pi - \mathrm{M}) \tag{10}$$

$$g_3 = \frac{r}{4}(\Pi + \mathrm{M}) \tag{11}$$

$$g_4 = \frac{1}{4}(1-r)(\Pi + \mathrm{M}) \tag{12}$$

$$\eta_1 = \frac{h^2 r}{4}(3\mathrm{M} - \Pi) \tag{13}$$

$$\eta_2 = \frac{h^2 (1-r)}{4}(3\mathrm{M} - \Pi) \tag{14}$$

$$\tau = \frac{b_2}{g_2} = \frac{b_4}{g_4} = \frac{\gamma_2}{\eta_2} \tag{15}$$

$$\tau = \frac{1-r}{2c_p \alpha} \tag{16}$$

where $\tau$ is the relaxation time, and the attenuation, $\alpha$, for the viscoelastic matrix may be computed as a function of frequency, using the attenuation coefficient in Table 1.

In this study, the fibers as well as the matrix are modeled using the MSDLM for modeling convenience, with different model parameters, though it may be natural to use the MSLM for fibers. Table 2 lists the values of the MSDLM parameters for both the epoxy matrix and graphite fiber, computed by using eqns. (9) through (16) and Table 1. Note that five different values are listed in Table 2 for $\tau$ for five frequencies, as found by using eqn. (16) and Table 1; these five frequencies are the center frequencies of the five ultrasonic probes to be used in this work (see Sections 3.1 and 3.2 below). The dashpot coefficients, $b_2$, $b_4$ and $\gamma_2$, in Fig. 4(b) may be computed from eqn. (15) once the spring constants and the relaxation time are known. Finally, it should be added that ultrasonic probes are modeled in this work by modifying the probe models developed by Baek and Yim (2004) such that they are compatible with the MSDLM (Baek, 2007).

Table 2 Parameters of MSDLM used in present study

| Parameters | Matrix (epoxy) | Fiber (graphite) |
|---|---|---|
| $g_1$ [N/m] | 2.352 ($10^9$) | 9.980 ($10^9$) |
| $g_2$ [N/m] | 1.018 ($10^9$) | 0.0 |
| $g_3$ [N/m] | 1.279 ($10^9$) | 5.005 ($10^9$) |
| $g_4$ [N/m] | 0.554 ($10^9$) | 0.0 |
| $\eta_1$ [N·m/rad] | 16.07 ($10^{-3}$) | 2.341 ($10^{-3}$) |
| $\eta_2$ [N·m/rad] | 6.954 ($10^{-3}$) | 0.0 |
| $\tau$ [sec] | 1.5 MHz 2.122 ($10^{-6}$) | — |
| | 2.5 MHz 1.273 ($10^{-6}$) | |
| | 7.0 MHz 4.547 ($10^{-7}$) | |
| | 15.0 MHz 2.122 ($10^{-7}$) | |
| | 30.0 MHz 1.061 ($10^{-7}$) | |

## 3. Problems Simulated

### 3.1. Problem for Evaluation of Phase Velocities

Fig. 5 shows a schematic diagram of the ultrasonic test simulated in the present work for the evaluation of phase velocities. The dimensions of the specimen are, as shown in the figure, 7.07 mm by 5.30 mm. These small dimensions are to avoid excessive computation time; the MSDLM is more computation-time demanding than the MSLM because of the Runge-Kutta temporal integration involved. Yet, this size of specimen turned out to large enough for the purpose of the present work. The thickness of the specimen was set to D = 5.30 mm, which was the minimum value found to avoid the near field. The radius of all fibers is set to 8.8 micrometers for convenience of numerical modeling introduced in Section 2.3, which is similar to 10 micrometers assumed in Yang and Mal (1994).

The layers labeled 'absorbing boundary' at both sides of the specimen as shown in Fig. 5 are to eliminate spurious reflections from the specimen's side boundaries that are modeled there solely for limiting the computation domain. Each absorbing boundary is built as a set of vertical material layers that are modeled using the MSDLM with gradually increasing damping towards the outside of the specimen, which effectively absorbs all incoming waves and reflect virtually no waves back to the medium of interest.

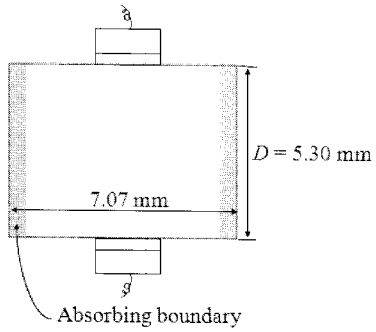


Fig. 5 Schematic diagram of simulation setup

For the problem depicted in Fig. 5, a through-transmission test is simulated. By measuring the time delay, Δt, between the wave signals received by the two probes, the phase velocities may be computed as

$$c_p \text{ or } c_s = \frac{D}{\Delta t} \tag{17}$$

Eqn. (17) may be used for both longitudinal (P) and vertically-polarized shear (SV) wave velocities by separately considering the cases of longitudinal and shear probes, respectively. Note that throughout this paper, all shear waves are vertically-polarized shear (SV) waves, not the horizontally-polarized shear (SH) waves, because the problem is two-dimensional without out-of-plane displacements. To this end, this study used the numerical model developed earlier for direct-contact transmitting ultrasonic probes (Baek, 2007) that can generate either longitudinal or shear wave, after some modifications to render it compatible with the MSDLM. The ultrasonic probes numerically modeled in this work have specifications listed in Table 3.

Table 3 Two probes assumed for numerical simulation for phase velocity evaluation

| Type | Mode | Size | Center frequency | -6dB bandwidth |
|---|---|---|---|---|
| Normal | P | 3.18 mm | 2.5 MHz | 2.5 MHz |
| | SV | | 1.5 MHz | 1.5 MHz |

### 3.2. Problem for Evaluation of Attenuation

Various test setups may be used for the measurement of ultrasonic wave attenuation. The test setup simulated in this work for this purpose is the same as that for phase velocity evaluation, shown in Fig. 5. In case of this direct contact between the probes and specimen, the attenuation may be computed as a function of frequency by (Kinsler et al., 1999)

$$\alpha(f) = \ln\left(A_{ref} / A_{spec}\right) / D \quad [\text{Np/m}] \tag{18}$$

where $A_{ref}$ and $A_{spec}$ are the amplitudes of

frequency spectra of the ultrasonic signals received after their transmission through a reference block and the specimen at hand, respectively.

The reference block assumed in this work is a rectangular block that is identical to the specimen except for the absence of fibers and damping, i.e. a homogenous block made of lossless epoxy (see Fig. 9(a)). Recall that even in this lossless reference block, ultrasonic waves will exhibit attenuation due to the spreading of beam. The reference block is thus used to measure this beam-spreading effect and subtract them from the attenuation in the specimen to obtain the attenuation solely due to the composite material.

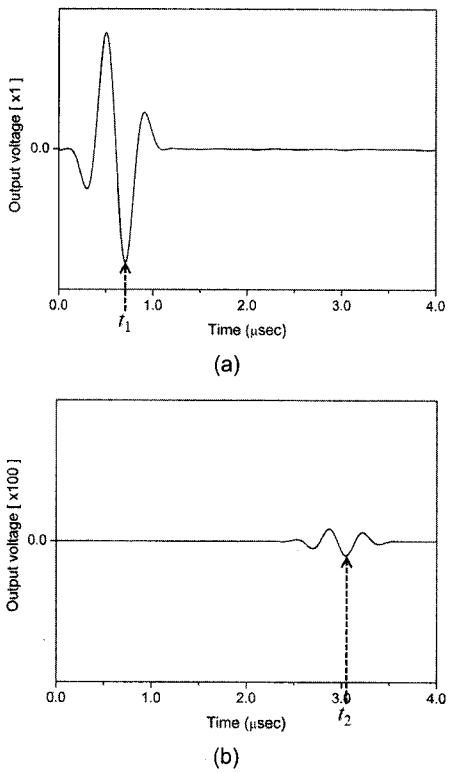


Fig. 6 Simulated received signals: (a) main-bang signal, (b) through-transmitted signal

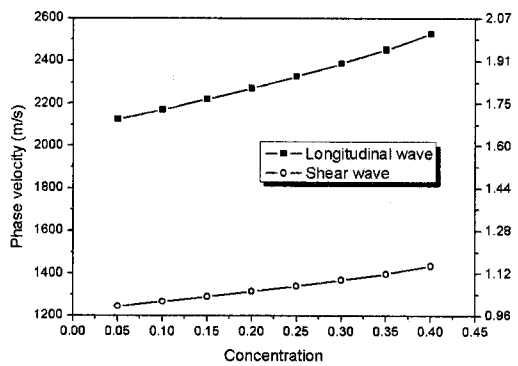


Fig. 7 Phase velocities versus fiber concentration

To be specific, if an identical probe is used, the wave amplitudes in the reference block and the specimen at a wave travel distance x may be written for a frequency component as

$$A_{ref}(x;f) = A_0 e^{-\alpha_r x} \tag{19}$$

$$A_{spec}(x;f) = A_0 e^{-\alpha_a x} \tag{20}$$

where $\alpha_r$ denotes the attenuation caused by the beam-spread effect, and $\alpha_a$ the apparent attenuation of the composite specimen, due to the combined effect of beam spreading, absorption, and wave scattering by fibers. Considering the test setup in Fig. 5, substituting x = D into eqns. (19) and (20), and combining the two resulting equations yield

$$\alpha(f) = \alpha_a(f) - \alpha_r(f) = \ln(A_{ref}(D)/A_{spec}(D))/D \ [Np/m] \tag{21}$$

which is the same as eqn. (18) because the left-hand side of eqn. (21), $\alpha = \alpha_a - \alpha_r$, is the sought attenuation of the composite material.

Finally, the probes listed in Table 3 have also been used for the purpose of attenuation evaluation, and three more probes with higher center frequencies (7, 15, 30 MHz) have been used in order to evaluate the attenuation over a broad range of frequency as will be presented below.

## 4. Numerical Results and Discussions

### 4.1. Phase Velocities

Typical examples of received signals for the simulated problem in Fig. 5 are shown in Fig. 6: (a) the 'main bang' signal received by the probe on the top boundary of the specimen, and (b) the through-transmitted signal received by the

other probe on the bottom boundary. As explained in the previous section, the wave arrival times, t1 and t2, are measured from the signals, and the phase velocities may be computed using eqn. (17) with $\Delta t = t_2 - t_1$. Following this procedure, the longitudinal and shear phase velocities have been computed for eight different fiber concentrations, i.e. fiber concentration ranging 0.05 ~ 0.4 at an increment of 0.05. The results are shown in Fig. 7.

Fig. 7 exhibits increasing phase velocities with increasing concentration, for both longitudinal and shear waves. This may be explained by the fact that the portion of the entire average wave path that falls within fibers, which exhibits faster wave speeds than the matrix, increases as the concentration increases. It may be noted that considering the center frequency of the probes used (see Table 3) and the fiber radius of 8.8 micrometers, the normalized shear wave number, $k_s a$, is about 0.067. This was deliberately set so for easy quantitative comparisons with the previous results provided for the same wave number (Yang and Mal, 1994).

The phase velocities at the lowest concentration of 0.05, observed from Fig. 7, are almost equal to those of the epoxy matrix, $c_p$ = 2060.6 m/s and $c_s$=1253.6 m/s, as may have been expected. In order to quantitatively compare the results in Fig. 7 with the Fig. 8 of Yang and Mal (1994), the phase velocities are also shown as normalized by the shear velocity of the matrix, 1253.6 m/s in this study (see the normalized scale along the right-hand side ordinate of Fig. 7). The comparison indicates that the phase velocities of both longitudinal and shear waves in Fig. 7 are in excellent agreement with the Fig. 8 of Yang and Mal (1994)-reproduced here as Fig. 8 for easy comparisons -from both qualitative and quantitative perspectives, except for a constant difference of 0.5 in the longitudinal wave velocities. (The authors believe that the entire curve for longitudinal wave velocity in the Fig. 8 of Yang and Mal(1994)

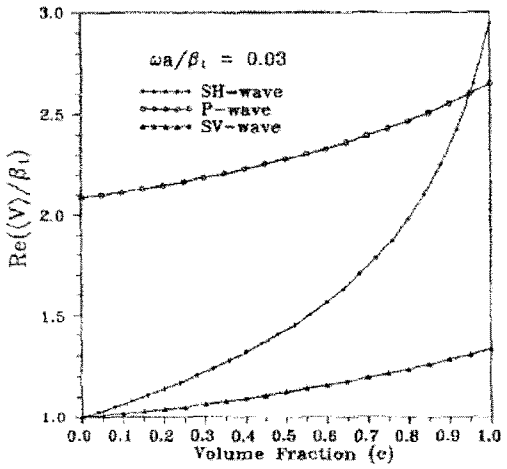


Fig. 8 Phase velocity versus concentration for graphite-epoxy composites at low frequencies (Fig. 8 of Yang and Mal, 1994)

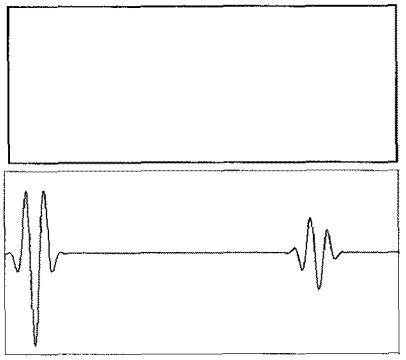

(a)

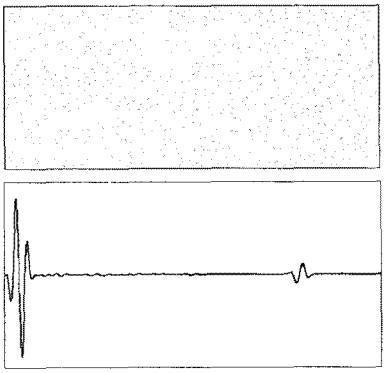

(b)

Fig. 9 Schematic diagrams and received signals from simulation for attenuation evaluation: (a) lossless matrix and simulated signal obtained using MSLM, (b) composite and simulated signal obtained using MSDLM

was erroneously shifted up about 0.5 on the normalized scale because the curve as it is does not retrieve the matrix phase velocity at the lowest concentration of 0.05, which it should.)

### 4.2. Attenuations

Fig. 9 shows typical examples of simulated received signals that have been used for the evaluation of attenuations following the procedure explained in the Section 3.2. Fig. 9(a) shows the lossless homogeneous matrix medium modeled using the MSLM, and the simulated received signal (the reference signal) from the homogeneous medium. On the other hand, Fig. 9(b) shows the composite medium modeled using the MSDLM and the corresponding simulated signal.

By applying eqn. (21) to such simulated signals, we have obtained the attenuation for the longitudinal and shear waves of the composite as functions of frequency, for two fiber concentrations of 0.05 and 0.4. The results for longitudinal waves are shown in Fig. 10, and those for shear waves in Fig. 11, as functions of normalized frequencies, $k_pa$ and $k_sa$. In both figures, the unit, Np/m in eqn. (21), has been converted to another unit, dB/cm, for easy comparison with the results in the literature.

Both Figs. 10 and 11 generally agree with

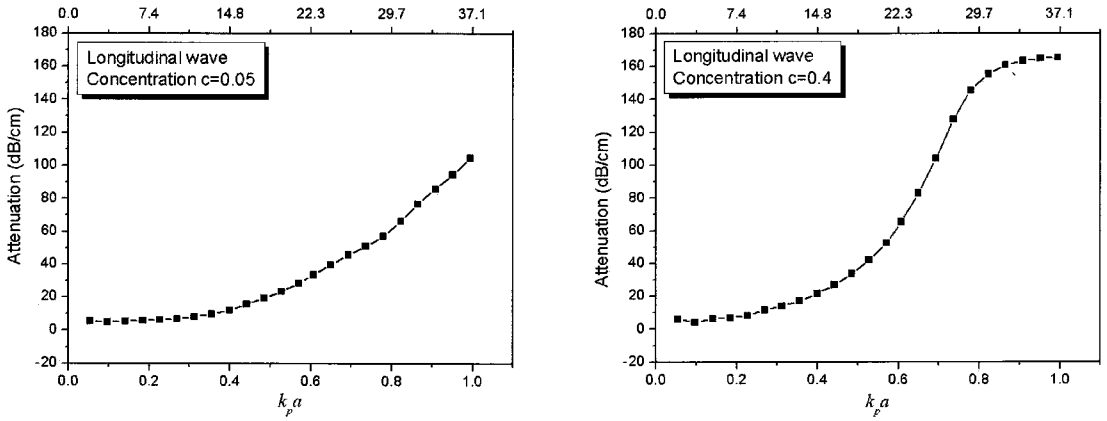


Fig. 10 Attenuation of longitudinal wave versus dimensionless frequency at fiber concentrations of (a) 0.05, and (b) 0.4

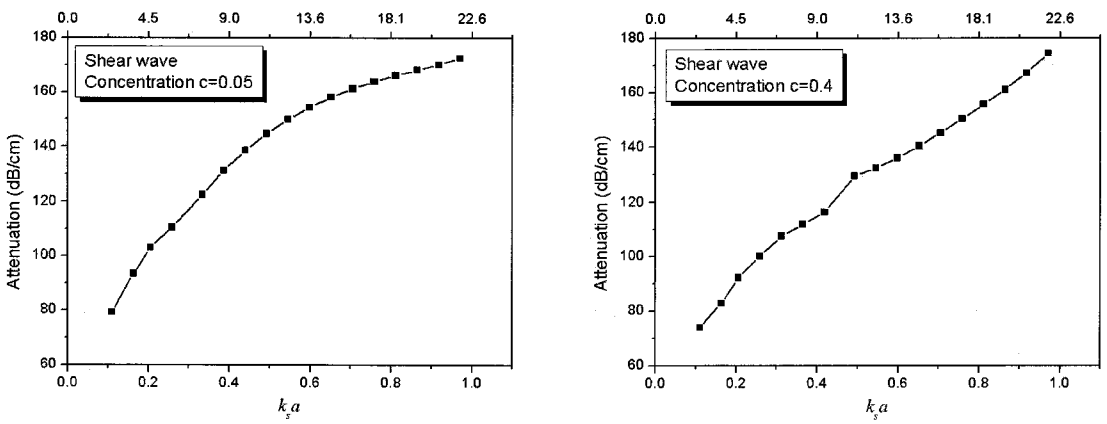


Fig. 11 Attenuation of shear wave versus dimensionless frequency at fiber concentrations of (a) 0.05, and (b) 0.4

the corresponding results in the literature (Varadan et al., 1986; Yang and Mal, 1994; Yang, 2003) in that the attenuation increases with frequency. Also, for the longitudinal wave attenuation (Fig. 10), the case of high concentration, 0.4, is observed to generally exhibit higher increase rate of attenuation than the case of low concentration, 0.05, which agrees with the Fig. 2(b) of Yang (2003).

It is also observed from Figs. 10 and 11 that attenuations in the case of higher fiber concentration are lower than or comparable to those in the case of lower concentration, for both longitudinal and shear waves (particularly so for shear waves). This observation may contradict with one's initial expectation, yet it may be explained as below by recalling that attenuation of ultrasonic waves in composite materials may be attributed to wave absorption due to material damping (only in the matrix, here), and wave scattering from fibers. Wave scattering however may not occur quite actively in the lower frequency region in Figs. 10 and 11, so the attenuation in this region is mostly due to the wave absorption in epoxy matrix. Therefore, in this lower frequency region in Figs. 10 and 11, attenuations are greater in the case of lower fiber concentration (meaning relatively more epoxy content) than in the case of higher concentration. As the frequency increases, wave scattering from fibers become more active, leading to greater attenuation with higher concentration in the longitudinal wave case (Fig. 10). Yet, in the case of shear waves, wave scattering does not become active enough to override the absorption effects within the studied frequency range $k_s a \leq 1.0$ (Fig. 11).

Though agreements have been found in general aspects between the attenuations obtained in the present work and the corresponding results in the literature, many discrepancies in detailed aspects have also been found; for example, steep increase of attenuation in higher frequency range often reported in the literature is not observed in the numerical results of this paper, and the numerical values of attenuation do not show quantitative agreements. However, considering the fact that the attenuation results in the literature themselves do not agree with each other (unlike the phase velocity results), the attenuation results obtained in this work may be considered to agree reasonably well with the literature in regard to their commonly valid characteristics.

## 5. Conclusions

In this work, graphite-epoxy fiber-reinforced composite has been numerically modeled using the mass-spring-dashpot lattice model (MSDLM). To this end, the fibers have been randomly distributed with a constraint that no pair of fibers may lie within a certain distance determined commensurate with the fiber concentration. The lossy epoxy matrix has been modeled using the MSDLM with pertinent damping parameters whereas the lossless graphite fibers with no damping.

By numerically simulating transmission of ultrasonic waves through the thus modeled composite medium, the phase velocities and attenuations of the average longitudinal and shear ultrasonic waves in the composite have been reported for various fiber concentrations or for various frequencies. The phase velocities obtained using the present approach have been observed to agree well with the corresponding results in the literature. The evaluated attenuations, however, showed discrepancies from the results in the literature with respect to detailed aspects though they agree well with each other in the general behavior.

The authors believe that the present work may be more accurate than other results in the literature because the present approach models the composite as it is or as closely as possible whereas other studies in the literature are based on hypothetical, mathematical models developed with artificial assumptions. This argument may

be corroborated by the wide discrepancies observed among the attenuation results, in the literature, based on different models. In order to verify this argument, it is desired to conduct experiments, and compare the results with the numerical results obtained by the present method.

## Acknowledgements

This work was supported by Grant No. R01-2005-000-10395-0 from the Basic Research Program of the Korea Science & Engineering Foundation, and by 2006 Hongik University Research Fund.

## References

Baek, E. and Yim, H. (2004) Development of an Ultrasonic Testing Simulator Using the Mass-Spring Lattice Model, Review of Quantitative Nondestructive Evaluation, Vol. 23, pp. 67-73

Baek, E. (2007) Numerical Modeling of Ultrasonic Testing for Anisotropic Elastic Welds and Biological Tissues, Ph. D. Thesis, Hongik University

Biwa, S., Yamamoto, S., Kobayashi, F. and Ohno, N. (2004) Computational Multiple Scattering Analysis for Shear Wave Propagation in Unidirectional Composites, International Journal of Solids and Structures, Vol. 41, pp. 435–457

Bose, S. K. and Mal, A. K. (1973) Longitudinal Shear Waves in a Fiber-reinforced Composite, International Journal of Solids and Structures, Vol. 9, pp. 1075-1085

Bose, S. K. and Mal, A. K. (1974) Elastic Waves in a Fiber-reinforced Composite, Journal of the Mechanics and Physics of Solids, Vol. 22, pp. 217-229

Christensen, R. M. and Lo, K. H. (1979) Solutions for Effective Shear Properties in Three Phase Sphere and Cylinder Models, Journal of the Mechanics and Physics of Solids, Vol. 27, pp. 315-330

Datta, S. K., Ledbetter, H. M., Shindo, Y. and Shah, A. H. (1988) Phase Velocity and Attenuation of Plane Elastic Waves in a Particle-Reinforced Composite Medium, Wave Motion, Vol. 10, pp. 171-182

Dorighi, J., Krishnaswamy, S. and Achenbach, J. (1997) A Fiber Optic Ultrasonic System to Monitor the Cure of Epoxy, Research in Nondestructive Evaluation, Vol. 9, pp. 13-24

Foldy, L. L. (1945) The Multiple Scattering of Waves I. General Theory of Isotropic Scattering by Randomly Distributed Scatterers, Physical Review, Vol. 67, No. 3&4, pp. 107-119

Kinsler, L. E., Frey, A. R., Coppens, A. B. and Sanders, J. V., (1999) *Fundamentals of Acoustics*, 4th ed., John Wiley & Sons

Kolsky, H. (1963) *Stress Waves in Solids,* Dover, New York

Pao, Y. H. and Mow, C. C (1963) Scattering of Plane Compressional Waves by a Spherical Obstacle, Journal of Applied Physics, Vol. 34, No. 3, pp. 493-499

Sayers, C. M. (1980) On the Propagation of Ultrasound in Highly Concentrated Mixtures and Suspensions, Journal of Physics D: Applied Physics, Vol. 13, pp. 179-184

Sayers, C. M. and Smith, R. L. (1983) Ultrasonic Velocity and Attenuation in an Epoxy Matrix Containing Lead Inclusions, Journal of Physics D: Applied Physics, Vol. 16, pp. 1189-1194.

Thomas, A. F. (2006) Lattice Modeling of Ultrasonic Nondestructive Evaluation of Attenuat-

ing Materials, Ph. D. Thesis, M.I.T.

Twersky, V. (1962a) On the Scattering of Waves by Random Distributions I. Free-space Scatterer Formalism, Journal of Mathematical Physics, Vol. 3, No. 4, pp. 700-715

Twersky, V. (1962b) On Scattering of Waves by Random Distributions II. Two-Space Scatterer Formalism, Journal of Mathematical Physics, Vol. 3, No. 4, pp.724-734

Varadan, V. K., Varadan,V. V. and Pao, Y. H. (1978) Multiple Scattering of Elastic Waves by Cylinders of Arbitrary Cross Section. I. SH Waves, Journal of Acoustical Society of America, Vol. 63, No. 5, pp. 1310-1319

Varadan, V. K., Ma, Y. and Varadan,V. V. (1986) Multiple Scattering of Compressional and Shear Waves by Fiber-Reinforced Composite Materials, Journal of Acoustical Society of America, Vol. 80, No. 1, pp. 333-339

Waterman, P. C. and Truell, R. (1961) Multiple Scattering of Waves, Journal of Mathematical Physics, Vol. 2, No. 4, pp. 512-537

Willis, J. R. (1980a) A Polarization Approach to the Scattering of Elastic Waves-I. Scattering by a Single Inclusion, Journal of the Mechanics and Physics of Solids, Vol. 28, pp. 287-305

Willis, J. R. (1980b) A Polarization Approach to the Scattering of Elastic Waves-II. Multiple Scattering from Inclusions, Journal of the Mechanics and Physics of Solids, Vol. 28, pp. 307-327

Yang, R. B. and Mal, A. K. (1994) Multiple Scattering of Elastic Waves in a Fiber-Reinforced Composite, Journal of the Mechanics and Physics of Solids, Vol. 42, No. 12, pp. 1945-1968

Yang, R. B. (2003) A Dynamic Generalized Self-Consistent Model for Wave Propagation in Particulate Composites, Journal of Applied Mechanics, Vol. 70, pp. 575-582

Yim, H. and Sohn, Y. (2000) Numerical Simulation and Visualization of Elastic Waves Using Mass-Spring Lattice Model, IEEE Transactions on Ultrasonics, Ferroelectrics and Frequency Control, Vol. 47, No. 3, pp. 549-558,

Yim, H. and Choi, Y. (2000) Simulation of Ultrasonic Waves in Various Types of Elastic Media Using the Mass Spring Lattice Model, Materials Evaluation, Vol. 58, pp. 889-896

Yim, H. and Lee, C. (2002) Quantitative Accuracy of the Mass-spring Lattice Model in Simulating Ultrasonic Waves, Review of Quantitative Nondestructive Evaluation, Vol. 21, pp. 152-156

Yim, H. and Baek, E. (2002) Two-Dimensional Numerical Modeling and Simulation of Ultrasonic Testing, Journal of the Korean Society for Nondestructive Testing, Vol. 22, No. 6, pp. 649-658

Yim, H. and Baek, E. (2004) Modeling of Transmitting and Receiving Ultrasonic Probes for Use with the Mass-Spring Lattice Model, Key Engineering Materials, Vol. 270-273, pp. 384-389